

Article

Case Study of Dam Overtopping from Waves Generated by Landslides Impinging Perpendicular to a Reservoir's Longitudinal Axis

Netsanet Nigatu Tessema ^{1,*}, Fjóla G. Sigtryggsdóttir ², Leif Lia ² and Asie Kemal Jabir ¹

¹ School of Civil and Environmental Engineering, Addis Ababa Institute of Technology, P. O. Box 385, Addis Ababa 1000, Ethiopia

² Department of Civil and Environmental Engineering, Norwegian University of Science and Technology, 7491 Trondheim, Norway

* Correspondence: Netsanet.nigatu@aait.edu.et; Tel.: +251-913-77-15-74

Received: 29 May 2019; Accepted: 25 June 2019; Published: 15 July 2019



Abstract: Landslide-generated impulse waves in dammed reservoirs run up the reservoir banks as well as the upstream dam slope. If large enough, the waves may overtop and even breach the dam and cause flooding of the downstream area with hazardous consequences. Hence, for reservoirs in landslide-prone areas, it is important to provide a means to estimate the potential size of an event triggered by landslides along the reservoir banks. This research deals with landslide-generated waves and the overtopping process over the dam crest in a three-dimensional (3D) physical model test, presenting a case study. The model set-up describes the landslide impacting the reservoir in a perpendicular manner, which is often the case in natural settings. Based on the experimental results, dimensionless empirical relations are derived between the overtopping volume and the governing parameters, namely the slide volume, slide release height, slide impact velocity, still-water depth, and upstream dam face slope. Predictive relations for the overtopping volume are presented as applicable for cases relating to the specific model set-up. Measured overtopping volumes are further compared to a two-dimensional (2D) case reported in the literature. An important feature regarding the overtopping process for the 3D case is the variation in time and space, resulting in an uneven distribution of the volume of water overtopping the dam crest. This observation is made possible by the 3D model set-up, and is of value for dam safety considerations as well as for foundation-related issues, including erosion and scouring.

Keywords: landslide-generated wave; dam overtopping; physical model; overtopping volume; impulse wave

1. Introduction

Dam sites suitable for impounding of a reservoir are often found in mountainous regions or highlands, often in narrow valleys or canyons (see Figure 1). Mountain slopes are generally susceptible for landslides, including rockslides. There are infamous cases of a landslide impinging reservoirs, in turn generating impulse waves overtopping the dam with catastrophic consequences downstream. This includes the Vajont dam tragedy in 1963 where nearly 2000 fatalities occurred [1]. The general process describing such events has been grouped into three phases [2]: (1) slide impact with wave generation; (2) wave propagation with wave transformation; and (3) run-up of the impulse wave and overtopping of a dam (see Figure 2). However, a dam is not overtopped if the wave run-up height is lower than the freeboard f , the elevation difference between the dam crest, and the reservoir still-water level, when the landslide impinges. Still, mountainous slopes surrounding a dam reservoir poses a threat to dam safety. Consequently, a mean of estimating the associated hazard from landslide waves

overtopping a dam is of importance. In such an evaluation, the reservoir settings, such as the geology and topography, are important. The shape of a reservoir in a narrow mountain valley is usually longer than its width (see Figure 1), and thus with a potential landslide threat from the mountain slopes along the length of the reservoir. In other words, a potential landslide may fall from these mountain slopes, i.e., approximately perpendicular to the reservoir’s longitudinal axis (see e.g., Figure 2b).



Figure 1. Mountain reservoir in Aurland Municipality Norway (Photo from E-CO Energi / Aerosport, with permission, 2019).

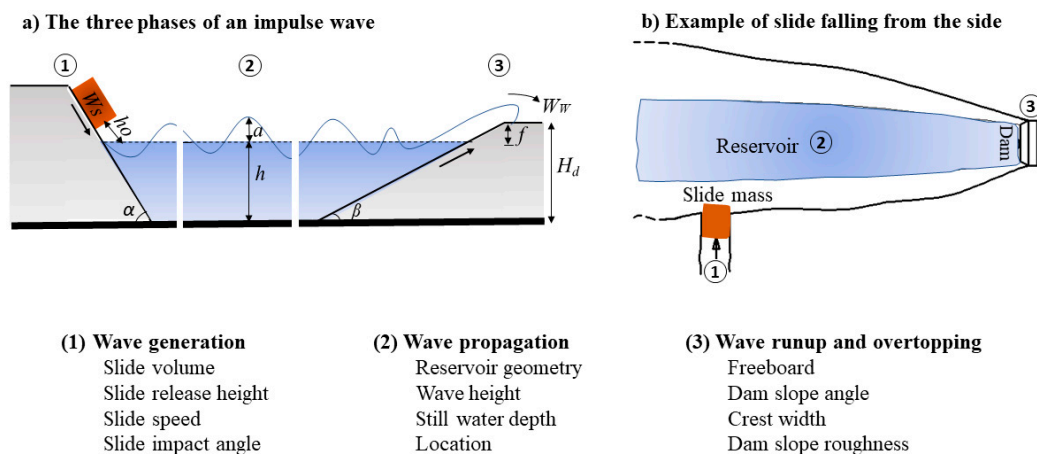


Figure 2. The three phases of landslide-generated waves with the relevant parameters for this study: (1) slide impact with wave generation; (2) wave propagation; and (3) wave run-up and overtopping of a dam; (a) a section showing the three phases based on Heller et al. [2]; (b) an example plan view of a reservoir.

Numerous experimental and numerical studies on landslide-generated waves (Phase 1 in Figure 2) are available. Many of those were conducted in flumes to investigate two-dimensional (2D) properties [3–7], while other studies [8–17] investigated the three-dimensional (3D) effects of landslide-generated tsunamis by considering wide reservoirs (3D water bodies) [11,16,17], as well as several geometries such as planar beaches and islands [8,12–14]. Those studies include landslides

modeled with granular and cobble material, and investigation into the effect of different landslide parameters such as landslide geometry and energy, on the wave generated. One recent relevant study is that of Evers [16], who investigated, for example, the effect of slide impact velocity, slide mass, slide impact angle, slide width, and still-water depth in 2D and 3D models. Evers [16] found that for the same slide mass (volume) the wave generation is influenced by the landslide geometry, with a wider landslide generating larger waves. Furthermore, he found that the initial wave amplitude and shape are influenced by the slide impact angle. These findings are mentioned here since in the current study the geometry of the slide is not directly considered in the formulations provided, and the slide impact angle is constant.

Only a few studies consider dam overtopping (Phase 3 in Figure 2) and include formulas for the overtopping volume based on wave and dam parameters. These studies are mainly those of Huber et al. [17] in the case of an erodible granular dam model, and Kobel et al. [18] as well as Müller [19] in the case of a solid, non-erodible dam model. The resulting formula for the overtopping volume is based on (2D) experimental tests. Kobel et al. [18] used rectangular prismatic water wave channels with solitary waves propagating directly towards a dam (set-up similar to shown in Figure 3b), thereby simulating waves generated by a landslide impinging from one end of the reservoir directly towards the dam. Kobel et al. [18] point out that the solitary wave type represents an extreme case.

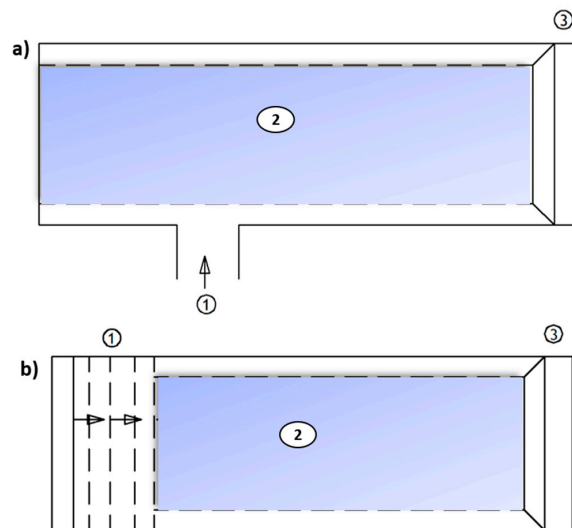


Figure 3. General layout of slide impact into a reservoir: 1 is the slide impact zone, 2 is the wave propagation zone and 3 the wave run-up and dam overtopping zone for (a) slide impacting from the side of a gorge; (b) solitary wave generated moving directly towards the dam's upstream face.

Depending on the geometry of a particular reservoir, the wave parameters can be computed with a 3D or 2D approach (e.g., [11,16]) and fed into a 2D run-up equation, such as provided by Kobel et al. [18], to obtain an estimate of the volume of water overtopping a dam. Heller et al. [2] discuss the effect of the reservoir shape with two extreme cases. The first case considers a long reservoir and a slide that impacts longitudinally into this reservoir. The second case considers that a slide mass can impact at any possible location into the reservoir and the slide width is less than the reservoir width. In the second case the reservoir geometry is such that the impulse wave can propagate radially and freely from the slide impact zone. In 3D settings the wave parameters depend on the wave propagation angle. The distribution of the overtopping wave along the dam crest, e.g., at the inner and outer flanks (see e.g., [2]), can be considered by dividing the dam crest in appropriate number of sections for the calculation of wave run-up and subsequent overtopping. However, the quality of the prediction would depend on the geometry of the reservoir and may be limited in the case of a very narrow reservoir as in the present study.

The above-mentioned studies do not directly investigate the 3D effect relating to narrow valleys and a landslide falling into a narrow dammed reservoir perpendicular to the reservoir's longitudinal axis, i.e., setups related to this shown in Figure 3a. Thus, further studies are required to investigate directly dammed reservoirs in narrow valleys with mountain slopes prone to landslide impinging perpendicular to the longitudinal axis of the reservoir (Figure 3a). The current study aims at shedding light on the mentioned 3D effect; however, application of the results must consider the limitations of the model set-up of this case study, as later described.

The current study continues an experimental study program initiated in 2014 with focus on landslide-generated waves resulting from lateral slides into a narrow reservoir, as well as the effect of different dam related parameters on wave overtopping. The study uses a 3D physical model that was extracted and modified from a model used by Lindstrøm et al. [20], to study rockslide generated waves into fjords. The same slide blocks are used as in Lindstrøm et al. [20], i.e., essentially modeling rockslides. Other researchers have studied landslide-generated impulse waves using granular deformable slides, e.g., Fritz et al. [21,22] used a 2D physical model and Mohammed and Fritz [23] used a 3D tsunami wave basin. Furthermore, there are studies available, e.g., Ataie-Ashtiani and Nik-Khah [7], Zweifel [24] and Heller and Spinneken [25], comparing the waves generated by granular and block slides. The findings of Zweifel [24] and Ataie-Ashtiani and Nik-Khah [7] was that rigid blocks (as in the present study), result in more extreme waves compared to granular slides. However, Heller and Spinneken [25] revealed that block slides can generate not only larger waves in a wave channel, but also identical or smaller waves than granular slides, depending on certain parameters or features. The identified influential parameters in this regard were the ratio of the slide width to the channel width, the slide front angle and the slope transition from the inclined landslide ramp used in the tests to the horizontal channel bottom. They explain the discrepancy from the previous studies that these parameters were not varied, and their effect thus not recognized.

The main objective of this article is to use the experimental data from the 3D laboratory scale test set-up to propose a formula for estimating the total volume of water overtopping a dam from impulse waves generated by a landslide impinging perpendicular to the reservoir longitudinal axis as shown in Figure 3a. An important part of this objective is to investigate the distribution of the overtopping volume along the dam crest, a feature that can, as described above, only be obtained indirectly through 2D modeling of previous studies essentially using experimental setups relating to that shown in Figure 3b. The experimental set-up of the present study has a fixed reservoir geometry as well as a fixed landslide ramp slope and location, which must be considered in the application of the results. The formula derived is dependent on both the landslide and dam parameters. The dam parameters considered, for the upstream slope and freeboard, relate e.g., to those relevant for embankment dams. However, the dam model used is non-erodible as in the case of Kobel et al. [18]. Considering this, an important further objective of this study is to compare, the overtopping volume measured in this study to predictions based on the formula of Kobel et al. [18].

In the following, the experimental set-up, instrumentation, and test program is outlined, followed by a description of the wave propagation and overtopping process. The experimental data is analyzed to obtain a formula for predicting the overtopping volume based on the landslide and dam parameters. The formula is obtained with data regression analysis resulting from test runs with systematic variation of slide, basin, and dam parameters such as the slide volume, slide release height, slide speed, wave amplitude and upstream dam face slope for cases with freeboard $f > 0$. Following this, the distribution of the overtopping along the dam crest is extracted. Finally, the measured overtopping volumes are compared to results using the prediction formula proposed by Kobel et al. [18]. The analysis chapter is supported with discussions on the limitations of the study and the results. Finally, the main conclusions are stated.

2. Methodology

2.1. Experimental Set-up

The main structural components of the physical model were: (i) a slide ramp on which slide blocks are released; (ii) the basin representing the reservoir; and (iii) an embankment dam (non-erodible) (Figure 4).

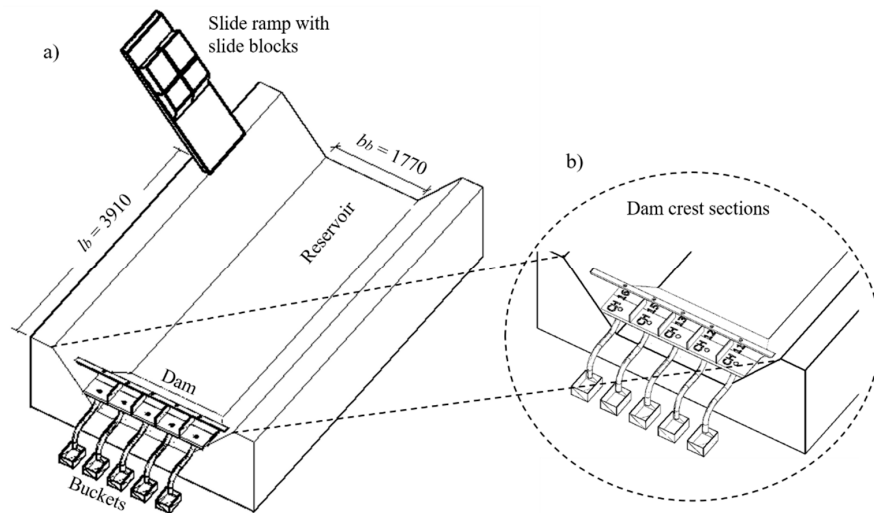


Figure 4. (a) Experimental set-up with the main components; slide, reservoir, dam and (b) ultrasonic sensors used for measuring the run-up height and buckets for collecting the overtopping water. The wave gauges, which were installed in the reservoir, are not shown on this figure.

The slide was modeled with blocks (see Figure 5) placed on a 2 m long slide ramp inclined at a constant angle of $\alpha = 50^\circ$, where it was possible to place rectangular blocks of different sizes and arrangements. This model represents a reservoir in a narrow valley formed by steep rock mountain slopes. Furthermore, the slide ramp was modeled as a natural extension of the sides of the model reservoir. The inclination of the slide ramp mainly affects the slide speed, along with the friction between the ramp and the blocks. The friction resistance was represented with a friction angle of about 25° . In this study, the slide speed was varied by using different slide release heights. The shapes and sizes of the blocks used in the experiments are shown in Figure 5. Different slide block arrangements were made for each test set-up. For each arrangement the blocks, impinging the water first, were tapered at an angle of 45° at the front to simulate a slide that has a smaller front and a larger body [26]. The slide blocks were attached to each other with chains, the sliding body was then attached to a steel panel with a hook. When the hook was removed, the blocks slid into the reservoir generating impulsive waves.

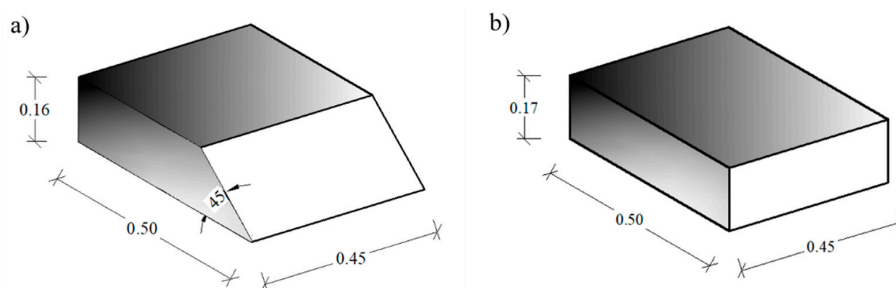


Figure 5. Rigid blocks used to model the landslide (measurement in m): (a) trapezoidal solid; (b) rectangular solid.

The reservoir was modeled with a fixed trapezoidal basin with sidewalls of water-resistant plywood covered with concrete paste to increase the roughness. It was 4.5 m long, 1.7 m wide at the bottom and 2.2 m at dam crest level, with a total reservoir capacity of 2.5 m³. The model dam was placed at one end of the reservoir with a constant height of $H_d = 0.32$ m. The model was conceptual and a scale of 1:190 has been selected relative to prototype, considering that this results in a moderate height of the prototype dam (60.8 m) and a range of landslide volumes from the blocks, representing medium sized slides (0.2 to 1 million m³) to large slides (1 to 5 million m³). At this scale (1:190) the model represents an 860 m long reservoir, 320 m wide at the bottom with a reservoir capacity of 17 Mm³.

Dams with upstream slopes of 1:1.5, 1:2 and 1:2.25 were used for the analysis representing embankment dams. The dam crest was divided into five different sections (labeled Channels (CH) 11 to 16 in Figure 4b) to measure the distribution of the overtopping volumes along the crest. The corresponding overtopping volume for each dam section was collected in five buckets with pipes of 100 mm diameter (see Figure 4b).

2.2. Instrumentation

Nine wave gauges of type 'DHI wave-meter 102E' were placed at the surface of the trapezoidal basin to measure the wave height at different locations. The principle of this wave meter is to measure the conductivity between two parallel electrodes partly immersed in water. In addition, there were five ultrasonic sensors (*mic+35/U/TC*) placed at the top of each dam section to measure the height of the water that overtopped the dam crest (see Figure 6). The water that overtopped the dam was collected in five calibrated buckets and recorded manually with an ultrasonic sensor. The initial level of each bucket was measured before the test and the water level rise after the test. The measurement was multiplied by a calibration factor to obtain the overtopping volume.

To measure the speed of the slide block, a rotational sensor (CH 10) was placed at the side of the slide ramp. It was connected to the rigid sliding blocks through a hook with a rope which unrolled together with the distance covered by the slide. A voltmeter recorded the voltage as the block slid down the ramp and the rope unrolled. A calibration factor was required to change the measured voltage into the distance covered by the slide. Then a time variable distance was used to extract the slide impact velocity considering the impact velocity is the maximum.

The data from the wave gauges, ultrasonic sensors and rotational sensors were collected in 'Agilent Measuring Manager program' with a sampling rate of 200 Hz.

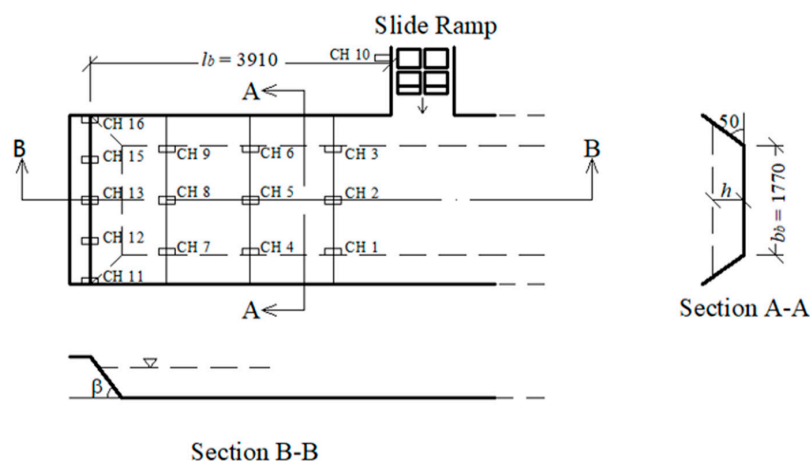


Figure 6. Planar view of sensors placement in the model set-up (measurements in mm).

2.3. Test Program

The overtopping of the dam by landslide-generated waves was investigated with parameters such as the landslide volume W_S , landslide release height h_O , landslide speed v_S , upstream dam slope

β and freeboard f . These parameters represent the input variables of the study provided as shown in Table 1. Four different types of block arrangements (2H, 2V, 4 and 6) with different length, width, and volume were used in the model as shown in Table 2 (Figure 7).

Table 1. Test program.

Scale	β (V:H)	f (m)	W_S (m ³)	h_O (m)
Model (1:190)	1: 2.25	0.024, 0.032	0.072, 0.074, 0.149, 0.225	0.5, 1, 1.5, 2
	1: 2	0.024, 0.032	0.072, 0.074, 0.149, 0.225	0.5, 1, 1.5, 2
	1: 1.5	0.024, 0.032	0.072, 0.074, 0.149, 0.225	0.5, 1, 1.5, 2
Prototype	-	4.5, 6	0.49, 0.51, 1.02, 1.54 (Mm ³)	95, 190, 285, 380

Table 2. Slide block characteristics in the model set-up.

Slide Characteristics	Block Arrangement			
	2H Blocks	2V Blocks	4 Blocks	6 Blocks
Slide length l_S (m)	0.50	1.08	1.08	1.66
Slide width b (m)	0.90	0.45	0.90	0.90
Shape ratio l_S/b (-)	0.56	2.40	1.20	1.84
Slide volume W_S (m ³)	0.072	0.074	0.149	0.225

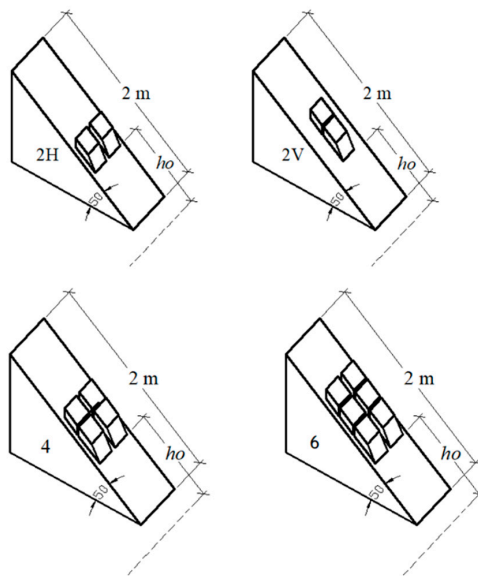


Figure 7. Arrangement of block configurations used in the tests with slide release height h_o parallel to the ramp slope and measured from the still-water level.

A constant dam height $H_d = 0.32$ m, crest width $b_c = 0.053$ m and length $l_c = 2.2$ m were used for the whole test series. However, three different upstream dam slopes were considered, i.e., $\beta = 24^\circ$ (1:2.25), 27° (1:2) and 34° (1:1.5) (see Figure 8). Additionally, two different freeboards were used: $f = 0.024$ m (still-water depth: $h = 0.296$ m) and 0.032 m ($h = 0.288$ m). Considering a scale of 1:190, the freeboard values correspond to 4.5 m and 6 m, respectively, associated with dams in Norway of high and very high consequences for the downstream area should the dam breach.

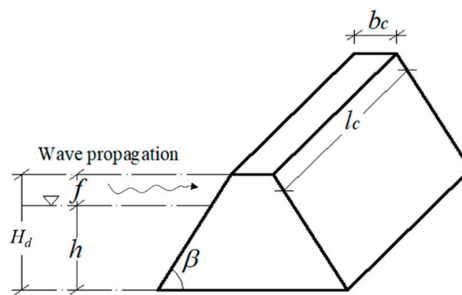


Figure 8. Definition sketch of a dam with the governing parameters.

66 experiments were conducted with varying slide, reservoir, and dam parameters. To check the test repeatability, each test with identical parameters was repeated three times and analyzed, hence a total of 198 tests have been conducted. All test data are given as the average of these three individual tests.

3. Wave Types, Propagation, and Overtopping Process

3.1. Wave Types and Propagation

Heller et al. [2] observed four transient impulse wave types for their 2D experiments in a wave channel: Stokes-like waves, cnoidal-like waves, solitary-like waves, bore-like waves, and all landslide-generated impulse waves may be allocated to one of these types. Each wave type (see Figure 9) has its own characteristics. The wave type influences for example the run-up height and wave force on the dam (see e.g., Heller and Hager [27]). Figure 10 provides an example of the wave profiles from all nine wave gauges on the reservoir, recorded during one of the 3D tests of this study (Test no. 185_2.25s_4.5_2H_200). The 3D waves generated in this study are more complex than in the 2D case; however, compared to the profiles of Figure 9, the recorded waves from all the tests conducted are Stokes-like waves, rather than any of the other wave types. Furthermore, investigation into selected waves revealed a ratio of wavelength to reservoir depth in the range of intermediate water waves.

A classification method to characterize landslide-generated waves is of interest and available in the literature. Heller et al. [2] identified the wave type product, $T = S^{1/3}M \cos[(6/7)\alpha]$, as a relevant number in this regard, where M is the relative slide mass ($M = m_s / (\rho_w b h^2)$, with m_s as the slide mass and ρ_w as the density of water) and S is the relative slide thickness ($S = s/h$, with s as the slide thickness). Previously, Wiegel et al. [3] and Noda [28] defined the slide Froude number F as the ratio of the falling box velocity v_s , and the shallow water waves celerity ($F = v_s / \sqrt{gh}$) and used F to identify the wave types produced by a falling block. Considering these numbers, Heller and Hager [27] defined wave type zones from the relationship between F and T for the 2D case. The boundaries of these wave type zones are plotted in Figure 11, where the axes show T versus F . Heller and Hager [27] observed for the 2D case mainly Stokes-like waves in the zone $T < 4/5F^{-7/5}$, mainly bore-like waves in the zone $T > 11F^{-5/2}$, and mainly cnoidal- and solitary-like waves in the intermediate zone $11F^{-5/2} \leq T \leq 4/5F^{-7/5}$. It is important to note that Heller and Hager [27] conducted granular slide tests, which may lead to different wave types under identical dimensionless parameters when compared to rigid slides such as in the present study. Heller and Spinneken [11] further investigated the wave types for the 3D case. They concluded from their 3D test results that the lower boundary ($T < 4/5F^{-7/5}$) remains characteristic also for 3D waves, whereas in the intermediate range both Stokes- and cnoidal-like waves were observed. Similar findings can be concluded from the 66 data points from the current 3D study plotted in Figure 11 and identified by the number of blocks used in the tests. The waves in all the tests conducted in the present study bear a resemblance to Stokes-like waves. This also applies to tests, involving 6-block as well as some of the 4-block tests that are plotted in Figure 11 in the intermediate zone defined for the 2D case for cnoidal- or solitary-like waves.

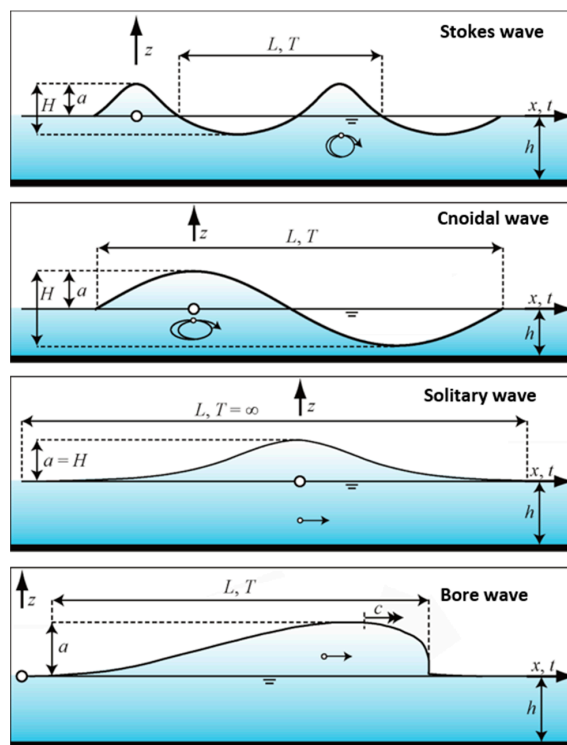


Figure 9. Idealized impulse wave types with the most important wave parameters (from Heller et al. [2], with permission from ETH, 2019).

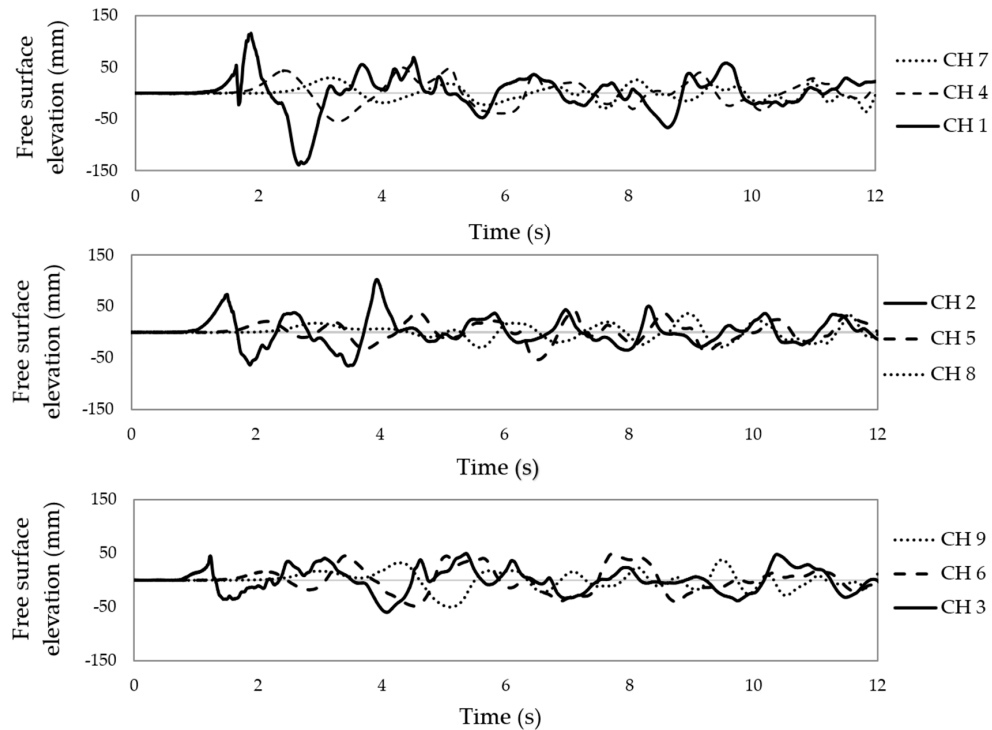


Figure 10. Wave profiles measured with the wave gauge sensors (see Figure 6 for the locations of the sensors) (Test no. 185_2.25s_4.5_2H_200).

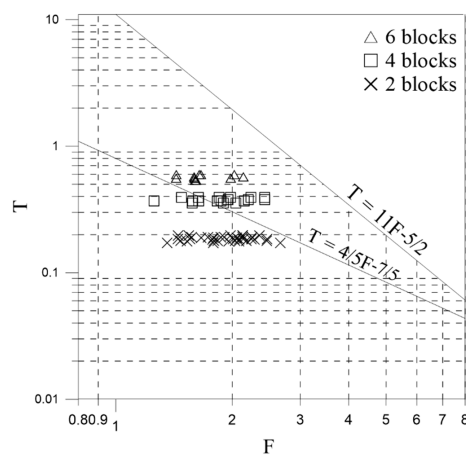


Figure 11. Plot of the wave type product T versus the Froude number F for the 3D tests conducted in the present study. All waves observed were Stokes-like. The boundaries provided are from Heller and Hager [27] observed for the 2D case using granular slides.

3.2. Wave Overtopping Process

Impulse waves induced by landslides impacting into reservoirs propagate and create wave run-up on the dam and shorelines. If the induced wave run-up exceeds the dam freeboard f the water overtops the dam and floods the downstream area. Kobel et al. [18] give a detailed description of the overtopping process for the 2D case and investigate the effect of the upstream slope, the freeboard and the dam width. Here, considering a 3D model, the focus is on variation in time and space of the overtopping waves, and thus the overtopping volume. During the overtopping process, the highest waves force a large volume of water over the crest in a short period of time, whereas the smaller waves may not produce any overtopping. The variation of the overtopping process in both time and space can be understood from Figure 12 presenting the time series obtained from all the sensors at the channels along the dam crest.

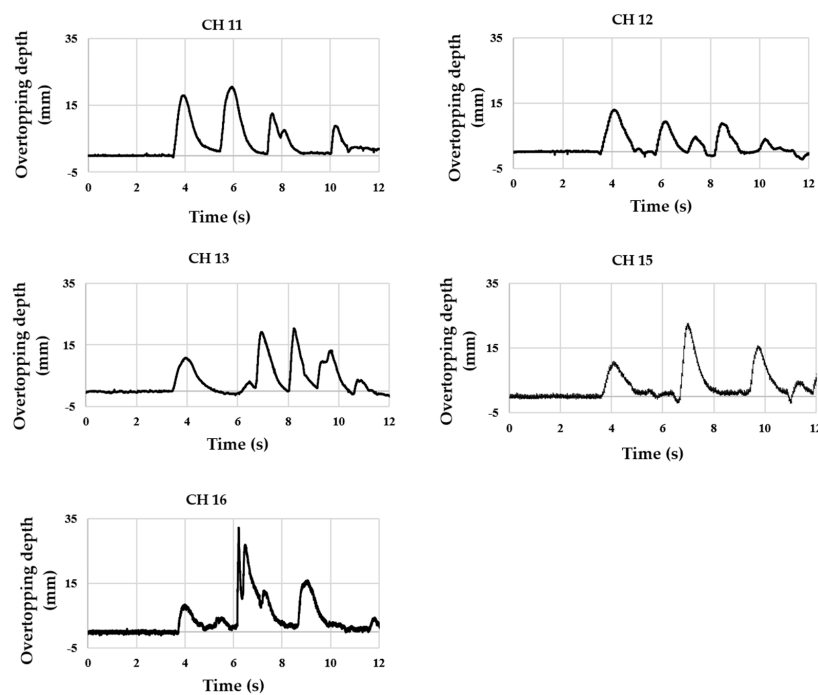


Figure 12. Overtopping depth (mm) versus time (s) over the five dam crest sections (see Figure 6 for the locations of the sensors) (Test no. 185_2.25s_4.5_2H_200).

4. Experimental Results

The experimental results are presented in this section. First, equations for the overtopping volume are derived for the experimental results. Furthermore, the uneven distribution of the overtopping volume is addressed.

4.1. Overtopping Volume

Once impulse waves are generated by landslides, they propagate and if large enough, overtop the dam thereby creating a certain volume of overtopping water. In this section, the relationship between the dimensionless parameters for the overtopping process will be assessed using an approach relating to e.g., that of Kobel et al. [18] and a predictive equation will be presented for the overtopping volume.

A dimensional analysis was conducted between the overtopping volume and the independent variables considering different landslide, reservoir, and dam geometries. Hence, the overtopping volume over the dam crest due to landslide-generated waves can be expressed as a function of:

$$W_w = f(W_s, h_o, g, v_s, h, \rho_w, a, l_b, b_b, \beta) \tag{1}$$

where W_w (m³) = overtopping volume, W_s (m³) = landslide volume, h_o (m) = landslide release height, g (m/s²) = gravitational acceleration, v_s (m/s) = slide impact velocity, h (m) = still-water depth, a (m) = wave amplitude, l_b (m) = reservoir length, b_b (m) = reservoir width and β (°) = dam front face angle.

In the model experiments a constant reservoir length, l_b and reservoir width, b_b were used; hence their effect is considered constant.

Applying Buckingham's π theorem, by selecting the repeating variables as; h , ρ_w and v_s , a relationship between dimensionless parameters is obtained:

$$\frac{W_w}{h^3} = f\left(\frac{W_s}{h^3}, \frac{h_o}{h}, \frac{v_s}{\sqrt{gh}}, \frac{a}{h}, \beta/90^\circ\right) \tag{2}$$

where the wave amplitude a is measured from the zero level to the maximum crest point. Equation (2) can be rewritten:

$$\frac{W_w}{h^3} = f\left(\frac{W_s}{h^3}, \frac{h_o}{h}, F, \varepsilon, \beta/90^\circ\right) \tag{3}$$

where $\varepsilon = a/h$ is the relative wave amplitude.

Conducting a power fit regression, a predictive equation is found for the relative overtopping volume:

$$\frac{W_w}{h^3} = 0.21 \left[\left(\frac{W_s}{h^3}\right) \left(\frac{h_o}{h}\right)^{0.43} (F^2)^{-0.08} \varepsilon^{0.04} (\beta/90^\circ)^{-0.01} \right] = 0.21E_1 \tag{4}$$

The following limitations apply: $2.67 < W_s/h^3 < 9.52$, $1.67 < h_o/h < 6.97$, $1.25 < F < 2.66$, $0.18 < \varepsilon < 0.73$ and $0.27 < (\beta/90^\circ) < 0.37$.

E_1 is the overtopping volume parameter considering the relative wave amplitude described as:

$$E_1 = \left[\left(\frac{W_s}{h^3}\right) \left(\frac{h_o}{h}\right)^{0.43} (F^2)^{-0.08} \varepsilon^{0.04} (\beta/90^\circ)^{-0.01} \right]; 2.9 < E_1 < 14.8 \tag{5}$$

Equation (4) includes a parameter relating to the wave crest; however, it also includes the relative slide volume which is influential for the wave amplitude as well as the landslide speed through F . However, the impact of ε , as well as $\beta/90^\circ$ and F , is quite small, indicating that these parameters can be neglected in the analysis of the overtopping volume W_w . The model set-up had a fixed distance from the dam to the slide impact zone. Thus, for this case a more direct relationship with the slide volume is possible by neglecting the wave parameter ε . Rearranging the parameters in Equation (4), for a direct

relationship between W_w and the other parameters on the right-hand side of the equation, results in a relationship for W_s , to the power of 1. Thus, the relationship between W_w and W_s is linear. For cases that can be related to the model set-up, and where no information about the wave properties are available, removal of the wave related parameter is advantageous for a clearer extraction of the relationship between overtopping volume and slide parameters. This further simplifies the process of roughly estimating the overtopping volume related to a known potential slide into a reservoir. Hence, in this study, an additional analysis was made for a predictive equation of overtopping volume excluding wave properties, such as ε . Accordingly, the overtopping volume prediction formula becomes

$$\frac{W_w}{h^3} = 0.17 \left[\left(\frac{W_s}{h^3} \right) \left(\frac{h_0}{h} \right)^{0.42} (F^2)^{-0.03} (\beta/90^0)^{-0.1} \right] = 0.17E_2 \tag{6}$$

The following limitations apply: $2.67 < W_s/h^3 < 9.52$, $1.67 < h_0/h < 6.97$, $1.25 < F < 2.66$ and $0.27 < (\beta/90^0) < 0.37$

E_2 is the overtopping volume parameter without considering ε described as:

$$E_2 = \left[\left(\frac{W_s}{h^3} \right) \left(\frac{h_0}{h} \right)^{0.42} (F^2)^{-0.03} (\beta/90^0)^{-0.1} \right]; 3.7 < E_2 < 17.8 \tag{7}$$

Based on the analysis the relative overtopping volume W_w/h^3 increases linearly and thus most significantly with the relative slide volume W_s/h^3 , but moderately with the relative landslide release height h_0/h . Furthermore, the impacts of F and $\beta/90^0$ are again quite small. The exponents for F and $\beta/90^0$ in Equation (6) are so small that they may be ignored in the analysis of the overtopping volume. When excluding these parameters, the exponent of the remaining parameters, W_s/h^3 and h_0/h , remains the same for W_s/h^3 , but only slightly reduces for h_0/h from 0.42 to 0.40. Furthermore, the constant in front of E_2 increases from 0.17 to 0.19. However, in the present study Equation (6) is considered for further analysis.

Figure 13 shows the correlation between measured relative overtopping volume W_w/h^3 and the overtopping volume parameters, E_1 and E_2 , each with $R^2 = 0.80$. To investigate and compare Equation (4) including, and Equation (6) excluding the relative wave amplitude, an analysis was performed for the value of overtopping volume comparing the power regression fits (expressed by $R^2 = 0.80$) between the measured values from the tests and the results from Equations (4) and (6), respectively. Figure 14 reveals large prediction errors for smaller measured overtopping volumes $W_w < 0.01 \text{ m}^3$ for both cases.

4.2. Overtopping Volume Distribution

Overtopping of a dam due to landslide-generated impulse waves is not uniform over the crest, for the case studied here with the landslide impinging along the reservoir’s longitudinal axis (Figures 3a and 4). The water overtops the left edge first, and then the right edge and lastly the whole dam crest length. Figure 15 presents the distribution of the overtopping volume along the dam crest showing that a large amount of water is collected at the right and left edges (CH 16 and CH 11, respectively) of the crest, on average about 28% each. On average a slightly higher volume is collected at the left side, i.e., opposite the landslide impact zone. Contrariwise, a smaller volume of water overtops the middle section of the dam crest (CH 12, CH 13 and CH15) (Figure 15). This uneven distribution of the overtopping wave and volume along the crest of the dam is due to the 3D modeling allowing reflected waves from the edges of the reservoir.

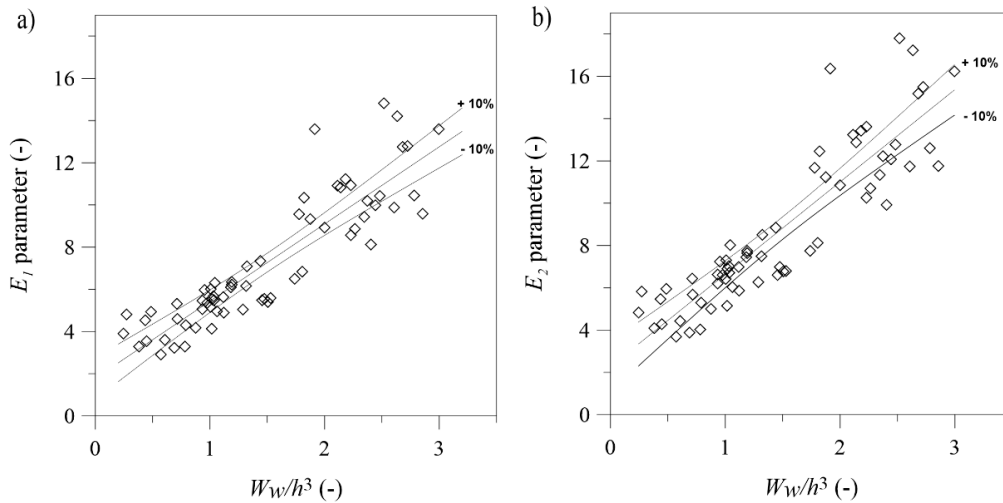


Figure 13. Relative maximum overtopping volume W_W/h^3 versus the wave overtopping volume parameter E_1 and E_2 with and without relative wave amplitude, respectively, as well as with 10% deviation (dashed line): (a) E_1 according to Equation (5) ($R^2 = 0.80$) and (b) E_2 according to Equation (7) ($R^2 = 0.80$).

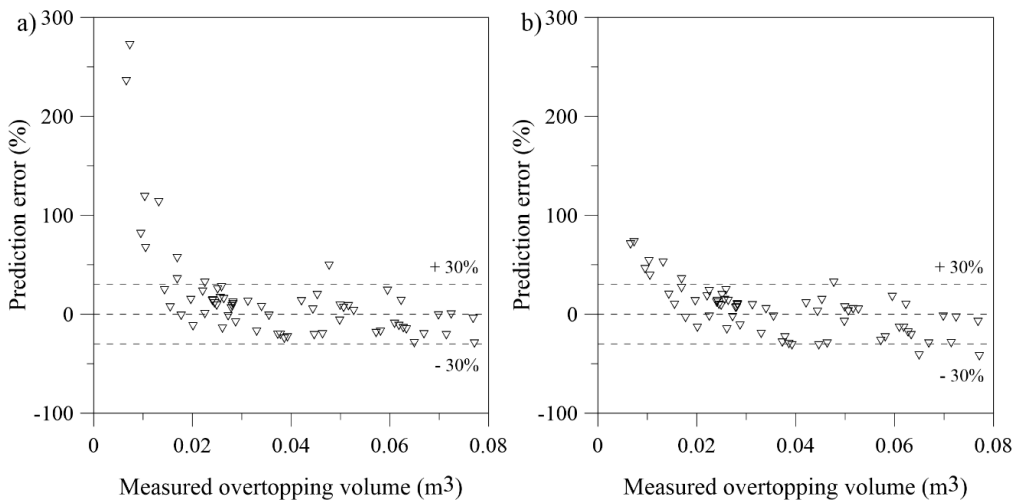


Figure 14. Prediction error for the measured overtopping volume: (a) predicted with Equation (4); (b) predicted with Equation (6).

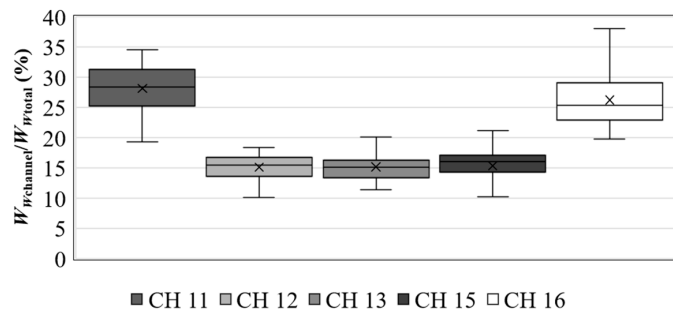


Figure 15. Overtopping volume distribution over the five dam crest sections (see Figure 6). The width of each channel is one fifth of the total dam crest length l_c .

5. Discussion

5.1. Comparison with Other Studies

Other studies include research dealing with dam overtopping due to impulse waves. For example, Müller [19] performed a series of 2D experiments considering the effect of the dam slope and crest width. He proposed an empirical equation for the overtopping volume per unit width, based on the run-up height. Recently Kobel et al. [18] studied dam overtopping due to solitary waves in a 2D laboratory scale set-up, relating to the case in Figure 3b, and presented an empirical equation for predicting the overtopping volume as

$$\frac{W_w}{b_b h^2} = 1.35 \left[\varepsilon \left(\frac{h}{H_d} \right)^{(2/\varepsilon)(\beta/90^0)^{0.25}} \left(\frac{a_w}{b_c} \right)^{0.12} \right]^{0.7} \quad (8)$$

where a_w is the effective wave amplitude defined as $a_w = h + a - H_d$.

It is of interest to compare results from Equation (8) to the measurements of the present study and Equations (4) and (6). Here, two approaches are considered. Approach 1 considers the largest wave amplitude recorded at wave gauge channels closest to the landslide impingement zone (CH 1, CH 2 and CH 3) and assumes that this is a solitary wave. Conversely, Approach 2 considers the wave amplitude recorded at the wave gauges closest to the dam (CH 7, CH 8 and CH 9) and calculates the overtopping volume of a single wave overtopping the dam crest for three sections, the dam inner flank and the outer flanks on each side.

Approach 1 considers that theoretically, the height of a solitary wave (and wave amplitude) as used by Kobel et al. [18] does not decrease and the 2D wave may propagate over unlimited distances without any change of shape. Hence, the parameters of this study are inserted into Equation (8) by assuming that a solitary wave, as in Kobel et al. [18], is generated by the landslide where it impinges the reservoir and that this wave overtops the dam. Thus, the maximum relative wave amplitude recorded in the wave generation zone is used in the calculations. This is a conservative approach, considering the model set-up and the 2D solitary wave type used by Kobel et al. [18]. The ranges of relative amplitudes ε used here by this approach are 0.18 to 0.73 which fall reasonably within the range 0.10 to 0.70 investigated by Kobel et al. [18]. To obtain the overtopping volume, the right-hand side of Equation (8) is multiplied by $b_b h^2$. The mean bottom channel width is used here as b_b .

Approach 2 considers that the waves generated in this study are not 2D solitary waves, but a 3D wave that decays as it propagates towards the dam at different wave propagation angles. Approach 2 provides the overtopping volume at the dam for a single wave. The ranges of ε used in the calculations by this approach are 0.10 to 0.34, which falls within the range 0.10 to 0.70 investigated by Kobel et al. [18] for the use of Equation (8). It should be noted that lower relative wave amplitudes are recorded in some of the tests at CH 7 to 9, but that no overtopping occurs at the respective dam crest sections for $\varepsilon < 0.08$ and $\varepsilon < 0.11$ in case of freeboards of 0.024 and 0.032 m, respectively.

In Figure 16 a comparison is made between predicted and measured overtopping volumes, where the predicted overtopping volume is calculated according to Equations (4) and (6) (deduced for the case in Figure 3a) as well as Equation (8) (deduced for the case in Figure 3b) for Approach 1 and 2. The measured overtopping volume is obtained from the model tests of the present study. Figure 16 demonstrates that as expected, the predictive equation of Kobel et al. [18], using a 2D solitary wave approach (Approach 1) overestimates the experimental data. On average the overestimation is more than twice the measured value. The overestimation factor, represented as the ratio between the predicted and measured overtopping, has a mean value of 2.63 with standard deviation of ± 1.09 . In comparison, Equations (4) and (6) extracted from the experimental data, on average, also slightly overestimate the experimental data by a factor of 1.13 and 1.18, respectively, and standard deviations of ± 0.5 and 0.48, respectively.

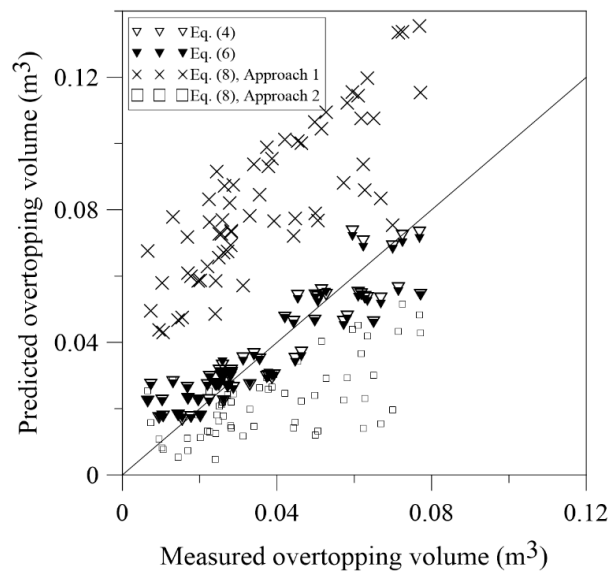


Figure 16. Predicted overtopping volume versus the total overtopping volume measured in the model tests (in m^3) of the present study. The total overtopping volume is predicted by Equations (4) and (6) of the present study and the overtopping volume from a solitary wave using Kobel et al. [18]’s Equation (8) using Approach 1 and 2.

The two Approaches 1 and 2 for the application of Kobel et al. [18]’s Equation (8) are compared in Figure 16. The overtopping volume calculated using Approach 1 overestimates the experimental data while Approach 2 generally underestimates the overtopping volume. For Approach 2, the measured total overtopping volume versus the one predicted by Equation (8), has a mean value of 0.70 with a standard deviation of ± 0.53 . The tests that involve large landslide volumes of 4 or 6 blocks, and the highest release height in each case, all result in more than one wave overtopping the dam in the case study. Thus, for these tests the overtopping volume from Approach 2 considering only a single wave largely underestimates the measured total overtopping volume.

5.2. 3D Effects

Figure 16 compares results from studies representing the two cases illustrated in Figure 3, i.e., a 2D study using solitary waves through Approach 1, versus the present 3D study of landslide impinging perpendicular to the reservoir’s longitudinal axis and inducing a more complex wave field (Figure 10). Additionally, the 3D wave effects are considered for the 2D formulation with the Approach 2 described above. Figure 16 confirms the statement by Kobel et al. [18] that 2D solitary wave represents the extreme case, considering that the predicted overtopping volume is on average more than twice the experimental results in Approach 1 applying Equation (8). However, Figure 16 also demonstrates that given the relative wave amplitude close to the run-up zone as in Approach 2, the use of Kobel et al. [18]’s, Equation (8) may underestimate the total overtopping volume in cases of narrow reservoirs. Thus, in a risk assessment for the downstream area, threatened by the water overtopping a dam, the water volumes estimated by Equations (4) and (6) are more appropriate for cases as those illustrated in Figures 2a and 3a, but only if these cases can be represented by the physical model of this study (Figures 4 and 6). Approach 1 for the application of Equation (8) by Kobel et al. [18] is appropriate for cases as shown in Figure 3b in case of solitary waves, but is likely to give extreme values, and thus be on the safe side for the cases shown in Figure 3a. Conversely, the 3D Approach 2 to the application of Equation (8) is likely to underestimate the overtopping volume for reservoirs relating to this case study, particularly involving large landslides. Thus, for Approach 2, Equation (8) must be applied cautiously to cases of narrow reservoirs and large landslides because of the potential number of waves

overtopping the dam. Combined application of Approaches 1 and 2 for predictions by Equation (8) could be considered, but may give a wide range of potential overtopping volumes.

One important feature extracted from the present study of landslides impinging perpendicular to the longitudinal axis of the reservoir (Figure 3a) is the uneven distribution of the overtopping volume over the dam crest (Figure 15). Equations (4) and (6) provide the total volume of water overtopping the dam. However, from a dam safety perspective the distribution of this along the dam crest is of interest. This distribution can be estimated from Figure 15.

5.3. Limitations and Potential Practical Application

A major limitation of all studies on landslide induced waves overtopping dams is the lack of relevant field data to calibrate physical and numerical models. This is in addition to potential scale effects in physical models, and the simplifications inherent in all modeling, including arising from potential inaccuracies of the instruments. The results from the present study, and other similar ones, should only be used as an aid in risk assessment, assessment of mitigation measures and in decision making that is influenced by dam safety. Furthermore, when applying Equations (4) and (6) the limitations inherent in the fixed model set-up of the present study must be considered. This includes the fixed reservoir geometry, the fixed slope of the landslide ramp, as well as the fixed distance to the landslide ramp. Additionally, the formulation considers only the landslide volume but not the landslide geometry (see Figure 7 and Table 2), but for two slides of the same volume but a different geometry, the wider slide will produce a larger wave and somewhat a larger overtopping volume. Thus, when applying the formulas, the landslide block arrangement (Figure 7) used in the present study must be considered. Furthermore, the slide blocks used represent subaerial rockslides, i.e., those released above the water surface. The results from this study are likely to give extreme values for cases where the landslide extends into the reservoir.

Geological investigations in reservoir areas may identify a potential landslide or rockslide. From the ranges of estimates of the slide size and location in relation to the dam, the equations from this study can be selected for cases that can be represented by Figure 3a and the model set-up (Figures 4 and 6). Assuming the case of Figure 3a, estimation of the necessary parameters to insert into Equation (6) should be attainable, and the same applies to the dam related parameters. However, the estimation must consider the limitations of the fixed reservoir geometry and landslide location stated above. Furthermore, for cases represented by Figure 3a but with very different landslide location from the model set-up (Figures 4 and 6) the results of this study should be used cautiously, with full recognition of the fixed reservoir and landslide set-up. Conversely, the formulation by Kobel et al. [18] requires evaluation of 3D wave parameters (similar to Approach 2) and can then be applied to the more general case, but with caution, at least in the case of a narrow reservoir and a large landslide impinging perpendicular to the reservoir's longitudinal axis. However, the extreme case can be realized with Approach 1 for the use of Kobel et al. [18]'s Equation (8). In any case, the estimated total volume of water overtopping the dam can subsequently be used to realize the potential size of the event threatening the downstream area. However, a time factor is required for calculations of potential flooding of the downstream area (see e.g., Kobel et al. [18]), i.e., resulting in overtopping discharge values. This will be dealt with in a separate article.

The information on the uneven distribution of the overtopping volume may be of importance in assessments for both dam and foundation-related issues, including erosion and scouring. Furthermore, the assessments mentioned can help in decision making regarding the execution of a project in landslide-prone regions, as well as mitigation measures such as monitoring of the landslide, or restricted operation for example through requirements on a minimum freeboard.

6. Conclusions

The research presented deals with the 3D case of a dam overtopped by waves generated as a landslide impinges the reservoir perpendicular to its longitudinal axis (Figure 3a). The governing

parameters include the slide volume, landslide release height, landslide speed, slide Froude number, still-water depth, and upstream slope of the dam. In line with the main objective of the paper, an empirical data analysis has been conducted to arrive at Equations (4) and (6) predicting the total volume of water overtopping the dam, based on the fundamental governing variables. The result from the analysis highlights the dominant effect of the slide volume followed by the still-water depth and landslide release height whereas the effect of the upstream dam slope is small. Limitations for the trend equations are stated enabling rough predictions, also in cases where information on some of the parameters may be absent. Furthermore, limitations on the applicability relating to the fixed geometry of the set-up are highlighted.

In line with one of the main objectives of the paper, the experimental data was compared to results using prediction formula derived for the 2D case by Kobel et al. [18]. The comparison confirmed the statement by Kobel et al. [18] that their approach with a 2D solitary wave represents the extreme case, which for the case considered here through Approach 1, resulted in an average overestimation of the measured value by more than a factor of two. However, if the 3D decay of a single wave is considered, as in Approach 2, the prediction by Kobel et al. [18] 's equation generally underestimates the experimental data and may result in an undesirable underestimation in cases where the wave is generated by a large rock slide into a narrow reservoir. In these cases, it is important to estimate the potential number of waves overtopping the dam.

Equations (4) and (6) can, with consideration of the stated limitations, be used for predicting the total volume of water that will overtop a specific dam due to landslide-generated waves with given landslide and dam properties. However, in such an estimation it is of high importance to note the limitation of Equations (4) and (6) arising from the fixed model set-up, i.e., geometry of the basin, location of the landslide ramp, and that the landslide geometry is not considered. Still, the equations can then be used to realize roughly the size of the event threatening the downstream area due to potential landslide-generated waves. The results should only be used to support risk assessment, assessment of mitigation measures, and decision making that is influenced by dam safety.

The overtopping process was described by figures and a quantitative data analysis. One important feature extracted regarding the overtopping process for the 3D case is the variation in time and space (Figure 12) resulting in uneven distributions of the volumes of water overtopping the dam crest (Figure 15). This observation was made possible by the 3D model set-up and is of value for dam safety considerations as well as for foundation-related issues, including erosion and scouring.

Author Contributions: Conceptualization, N.N.T., F.G.S. and L.L.; Formal analysis, N.N.T.; Investigation, N.N.T.; Project administration and Supervision, F.G.S.; Writing, N.N.T.; Writing, review and editing, F.G.S.; Review and editing L.L. and A.K.J.

Funding: Norwegian Water Resources and Energy Directorate (NVE) Project 80051.

Acknowledgments: The support and cooperation of the Norwegian Water Resources and Energy Directorate (NVE) and Grethe Holm Midttømme in the associated study and research program at NTNU is gratefully acknowledged. The contribution of Kiflom W. Belete in the early model development and to technical issues is appreciated. The important contribution of Jochen Aberle in the development of the model, particularly in reducing model effects, is acknowledged. Furthermore, the contribution of Geir Tesaker and Joël Biedermann in the laboratory, and of Ermyas Tamene Haile in the 3D drawing of the model set-up is acknowledged. The first author would like to acknowledge the support from Addis Ababa University, School of Civil and Environmental Engineering, as well as from NTNU, Department of Civil and Environmental Engineering.

Conflicts of Interest: The authors declare no conflict of interest.

Notation

a (m)	wave amplitude;
a_w (m)	effective wave amplitude;
b (m)	slide width;
b_b (m)	reservoir width;
b_c (m)	dam crest width;
E (-)	overtopping volume parameter;
F (-)	Froude number;
f (m)	freeboard;
g (m/s ²)	gravitational acceleration;
h (m)	still-water depth;
h_o (m)	landslide release height;
H (m)	wave height;
H_d (m)	dam height;
l_b (m)	reservoir length;
l_c (m)	crest length;
l_s (m)	slide length;
M (-)	relative slide mass;
m_s (kg)	slide mass;
s (m)	slide thickness;
S (-)	relative slide thickness;
T (-)	wave type product;
v_s (m/s)	landslide speed;
W_S (m ³)	slide volume;
W_W (m ³)	overtopping volume;
α (°)	slide ramp angle;
β (°)	dam front face angle;
ε (-)	relative wave amplitude;
ρ_w (kg/m ³)	density of water;

References

1. Steven, N.W.; Simon, D. The 1963 landslide and flood at Vaiont reservoir Italy. A tsunami ball simulation. *Ital. J. Geosci.* **2011**, *130*, 16–26.
2. Heller, V.; Hager, W.H.; Minor, H.-E. *Landslide Generated Impulse Waves in Reservoirs: Basics and Computation*; VAW-Mitteilung 211; ETH: Zürich, Switzerland, 2009.
3. Wiegel, R.L. Laboratory studies of gravity waves generated by the movement of a submerged body. *Trans. Am. Geophys. Union* **1955**, *36*, 759–774. [[CrossRef](#)]
4. Kamphuis, J.W.; Bowering, R.J. Impulse waves generated by landslides. *Coast. Eng. Proc.* **1970**, *1*, 35. [[CrossRef](#)]
5. Watts, P. *Water Waves Generated by Underwater Landslides*. Ph.D. Thesis, California Institute of Technology, Pasadena, CA, USA, 1997.
6. Synolakis, C. Generation of long waves in laboratory. *J. Waterw. Port Coast. Ocean Eng.* **1990**, *116*, 252–266. [[CrossRef](#)]
7. Ataie-Ashtiani, B.; Nik-Khah, A. Impulsive waves caused by subaerial landslides. *Environ. Fluid Mech.* **2008**, *8*, 263–280. [[CrossRef](#)]
8. Briggs, M.J.; Synolakis, C.E.; Harkins, G.S.; Green, D.R. Laboratory experiments of tsunami runup on a circular island. *Pure Appl. Geophys.* **1995**, *144*, 569–593. [[CrossRef](#)]
9. Fritz, H.M.; Mohammed, F.; Yoo, J. Lituya Bay landslide impact generated mega-tsunami 50th anniversary. In *Tsunami Science Four Years after the 2004 Indian Ocean Tsunami: Part II: Observation and Data Analysis*; Cummins, P.R., Satake, K., Kong, L.S.L., Eds.; Pageoph Topical Volumes; Birkhäuser: Basel, Switzerland, 2009; pp. 153–175.
10. Di Risio, M.; Sammarco, P. Analytical modeling of landslide-generated waves. *J. Waterw. Port Coast. Ocean Eng.* **2008**, *134*, 53–60. [[CrossRef](#)]

11. Heller, V.; Spinneken, J. On the effect of the water body geometry on landslide–tsunamis: Physical insight from laboratory tests and 2D to 3D wave parameter transformation. *Coast. Eng.* **2015**, *104*, 113–134. [[CrossRef](#)]
12. Romano, A.; Di Risio, M.; Bellotti, G.; Molfetta, M.G.; Damiani, L.; De Girolamo, P. Tsunamis generated by landslides at the coast of conical islands: Experimental benchmark dataset for mathematical model validation. *Landslides* **2016**, *13*, 1379–1393. [[CrossRef](#)]
13. McFall, B.C.; Fritz, H.M. Physical modelling of tsunamis generated by three-dimensional deformable granular landslides on planar and conical island slopes. *Proc. R. Soc. A Math. Phys. Eng. Sci.* **2016**, *472*, 20160052. [[CrossRef](#)] [[PubMed](#)]
14. Bellotti, G.; Romano, A. Wavenumber–frequency analysis of landslide-generated tsunamis at a conical island. Part II: EOF and modal analysis. *Coast. Eng.* **2017**, *128*, 84–91. [[CrossRef](#)]
15. Di Risio, M.; Bellotti, G.; Panizzo, A.; De Girolamo, P. Three-dimensional experiments on landslide generated waves at a sloping coast. *Coast. Eng.* **2009**, *56*, 659–671. [[CrossRef](#)]
16. Evers, F. *Spatial Propagation of Landslide Generated Impulse Waves*; VAW-Mitteilung 244; ETH: Zürich, Switzerland, 2017.
17. Huber, L.E.; Evers, F.M.; Hager, W.H. Solitary wave overtopping at granular dams. *J. Hydraul. Res.* **2017**, *55*, 799–812. [[CrossRef](#)]
18. Kobel, J.; Evers, F.M.; Hager, W.H. Impulse wave overtopping at rigid dam structures. *J. Hydraul. Eng.* **2017**, *143*, 04017002. [[CrossRef](#)]
19. Müller, D.R. *Auflaufen und Überschwappen von Impulswellen an Talsperren*; VAW-Mitteilung 137; ETH: Zürich, Switzerland, 1995.
20. Lindstrøm, E.K.; Pedersen, G.K.; Jensen, A.; Glimsdal, S. Experiments on slide generated waves in a 1:500 scale fjord model. *Coast. Eng.* **2014**, *92*, 12–23. [[CrossRef](#)]
21. Fritz, H.M.; Hager, W.H.; Minor, H.-E. Landslide generated impulse waves. 1. Instantaneous flow fields. *Exp. Fluids* **2003**, *35*, 505–519. [[CrossRef](#)]
22. Fritz, H.M.; Hager, W.H.; Minor, H.-E. Landslide generated impulse waves. 2. Hydrodynamic impact craters. *Exp. Fluids* **2003**, *35*, 520–532. [[CrossRef](#)]
23. Mohammed, F.; Fritz, H.M. Physical modeling of tsunamis generated by three-dimensional deformable granular landslides: Landslide generated tsunamis. *J. Geophys. Res. Oceans* **2012**, *117*, C11015. [[CrossRef](#)]
24. Zweifel, A. *Impulswellen: Effekte der Rutschdichte und der Wassertiefe*; VAW-Mitteilung 186; ETH: Zürich, Switzerland, 2010.
25. Heller, V.; Spinneken, J. Improved landslide–tsunami prediction: Effects of block model parameters and slide model. *J. Geophys. Res. Oceans* **2013**, *118*, 1489–1507. [[CrossRef](#)]
26. Sælevik, G.; Jensen, A.; Pedersen, G. Experimental investigation of impact generated tsunami; related to a potential rock slide, Western Norway. *Coast. Eng.* **2009**, *56*, 897–906. [[CrossRef](#)]
27. Heller, V.; Hager, W.H. Wave types of landslide generated impulse waves. *Ocean Eng.* **2011**, *38*, 630–640. [[CrossRef](#)]
28. Noda, E. Water waves generated by landslides. *J. Waterw. Harb. Coast. Eng. Div.* **1970**, *96*, 835–855.

